Aerospace Science and Technology 101 (2020) 105844

Contents lists available at ScienceDirect

Aerospace Science and Technology

www.elsevier.com/locate/aescte

Analysis of energy system configuration and energy balance for stratospheric airship based on position energy storage strategy

Chuan Shan [a], Mingyun Lv [a], Kangwen Sun [b,c,*], Jian Gao [a]

[a] School of Aeronautic Science and Engineering, Beihang University, 37 Xueyuan Road, Beijing 100191, PR China
[b] Institute of Unmanned System, Beihang University, 37 Xueyuan Road, Beijing 100191, PR China
[c] Yunnan Innovation Institute, Beihang University, 8 Shibo Road, Kunming 650233, PR China

ARTICLE INFO

Article history:
Received 2 February 2020
Received in revised form 13 April 2020
Accepted 13 April 2020
Available online 28 April 2020
Communicated by Mehdi Ghoreyshi

Keywords:
Position energy storage strategy
Energy balance
Energy system configuration
Stratospheric airship

ABSTRACT

The renewable energy system is one of the critical factors affecting stratospheric airships to achieve the long-duration station-keeping mission. This paper proposes a position energy storage strategy to achieve regional station-keeping by adjusting the airspeed of day and night. Firstly, a curved PV array model considering thermal effects and power required model are established. Then the flight strategy model and energy management model are established, and the feasibility of the position energy storage strategy is analyzed through a case. The results show that the strategy can solve the energy shortage problem of airship at night during some time periods, and in the high-speed wind field, the endurance time is increased from 6.94 h to 49.51 h through the pre-stored position potential and initial electrical energy. Moreover, the impact of location energy storage strategies on energy system configuration is discussed. The result shows that using the PES strategy as the design basis can reduce the total mass of the energy system, which has more advantages in areas with higher irradiation energy density and higher wind speed.

1. Introduction

The stratospheric airships are aerostats that fly in the stratosphere, can be used for scientific observation, ground monitoring, and long-term communication tasks [1,2]. To achieve the long-term station-keeping mission, renewable energy systems are needed to provide continuous energy input to the propulsion, avionics, and load systems.

The renewable energy system is mainly composed of PV arrays, energy-storage batteries, and energy management systems [3]. Power is generated by PV arrays during the day to power propulsion and airship-borne systems, while excess energy is stored in energy storage batteries for electricity at night. At present, the conversion efficiency of PV arrays and the energy density of energy storage batteries are not high enough, which becomes one of the main factors restricting the flight time of stratospheric airships.

As the energy source of the airship, the layout of PV array, solar cell temperature, and conversion efficiency all affect output performance. Wang and Shi firstly proposed a numerical simulation model for curved solar arrays [4,5]. Li analyzed the effect of temperature on the output characteristics of PV arrays by establishing a thermal model of solar cells [6,7] Pande also conducted a similar study [8]. Du analyzed the impact of the loss of incident angle on the output capacity of PV array [9].

Since the photoelectric conversion efficiency of solar cells will not significantly improve in the short term [10], how to increase the output capacity of photovoltaic arrays on the surface of airships by other methods has become a research hotspot in recent years. The solar tracking device is an effective way to increase the output capability of PV arrays [11,12]. Lv designed a rotatable PV arrays system, which can increase the output of PV arrays by more than 40% [13,14]. Zhu analyzed the influence of the stratospheric airship attitude on the output of the PV array and proposed a strategy for the best yaw angle [15]. Zhang analyzed the attitude planning scheme of airship fixed-point station-keeping with a rotatable PV array [16].

The above research on the airship energy system focuses on increasing photovoltaic array capacity through some strategy. Energy balance between day and night is also essential to fulfill the mission requirements of the trans-month flight. The stratospheric wind field is relatively stable, with small changes in the short

* Corresponding author at: Institute of Unmanned System, Beihang University, 37 Xueyuan Road, Beijing 100191, PR China.
E-mail addresses: shanchuan@buaa.edu.cn (C. Shan), sunkw100@buaa.edu.cn (K. Sun).

https://doi.org/10.1016/j.ast.2020.105844
1270-9638/

term, but substantial differences in different latitudes [17]. In areas with high wind speeds, large-capacity energy storage batteries are necessary for station-keeping at a fixed point. Nevertheless, considering the actual load capacity of the airship, it is not feasible to have a high battery quality ratio. Therefore, finding other ways to store surplus solar energy is necessary.

Solar-powered aircraft generally use the potential energy of gravity to store solar energy by changing the flight altitude [18,19]. However, changing the cruising altitude caused a drastic change in the internal pressure of the airship, so this flight strategy is not suitable for stratospheric airships. For airships cruising at a constant altitude, adjusting the day and night flight speed is considered as an effective strategy to improve the endurance [20]. Yang proposed that by adjusting the power of the day and night propulsion system, the stratospheric airship's endurance can be dramatically increased [21]. Ozoroski also proposed a position energy concept to evaluate the station-keeping capability of the airship [2]. However, there are still few studies on how to use wind energy storage to achieve regional station-keeping under different wind field conditions.

This paper aims to improve the endurance performance of the airship in a specific wind field by optimizing the day and night energy distribution. The structure of this article is as follows: Section 2 introduces the curved PV array output model and the required power model. Then the flight strategy model and energy management model are established in Section 3. Based on these numerical models, the result and discussion are presented in Section 4. Finally, the conclusion is given in Section 5.

2. Renewable energy system model

2.1. Stratospheric irradiation model

Solar radiation consists of direct, reflected, and scattered radiation. Radiation reflected by clouds would not illuminate the PV array located in the upper part of the airship. Hence, the stratospheric airship radiation model consists of direct radiation and scattered radiation. The intensity of direct solar radiation I_{d0} can be expressed as:

$$I_{do} = \tau_h \cdot I_0 \cdot \left(\frac{1 + e_e \cdot cos(\theta_{day})}{1 - e_e^2}\right) \tag{1}$$

Where I_0 is the solar radiation intensity constant, 1367 W/m^2. e_e is the eccentricity of the Earth's orbit, which is 0.0016708 [22]. θ_{day} is the diurnal angle and can be expressed as:

$$\theta_{day} = 2\pi \cdot (d_n - N_r)/365.24 \tag{2}$$

Where d_n is the nth day of the year and N_r is a leap year correction term which can be calculated with:

$$N_r = 79.6764 + 0.2422 \cdot (year - 1985) - int\left(\frac{year - 1985}{4}\right) \tag{3}$$

Where τ_h is the atmospheric transparency, and the atmospheric transparency in the stratosphere can be defined by:

$$\tau_h = 0.5 \cdot (e^{-0.65 \cdot amr} + e^{-0.95 amr}) \tag{4}$$

$$amr = \frac{P_H}{P_0} \cdot [\sqrt{1229 + (614 \cdot sin(\theta_s))^2} - 614 \cdot sin(\theta_{HS})] \tag{5}$$

Where amr represents the air mass ratio. P_H is the pressure at the altitude of the airship, P_0 is the sea level pressure that has a reference value of 101330 Pa. As shown in Fig. 1, the formula of solar height angle θ_{Hs}, solar declination angle θ_d and solar hour angle θ_{hour} can be given by:

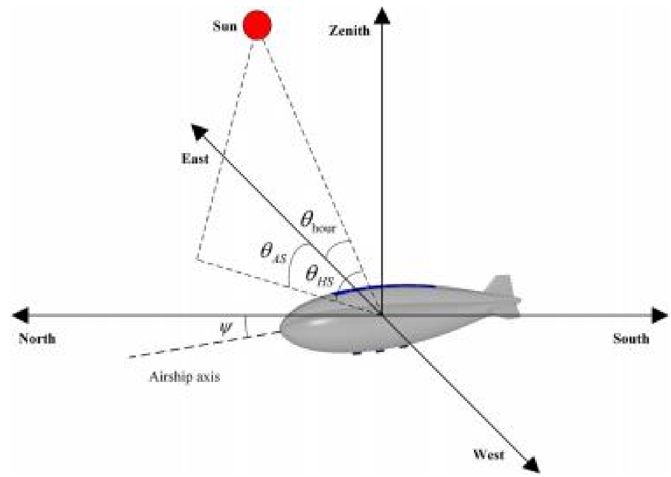

Fig. 1. Various angles of the solar irradiation.

$$\begin{aligned}
\theta_{HS} &= sin^{-1}(sin(\theta_d)sin(\phi) + cos(\theta_d)cos(\phi)cos(\theta_{hour})) \\
\theta_d &= [0.3723 + 23.2367 \cdot sin(\theta_{day}) + 0.1149 \cdot sin(2\theta_{day}) \\
&\quad - 0.1712 \cdot sin(3\theta_{day}) - 0.758 \cdot cos(\theta_{day}) \\
&\quad + 0.3656 \cdot cos(2\theta_{day}) + 0.0201 \cdot cos(3\theta_{day})] \\
\theta_{hour} &= 15 \cdot (t_n - 12) \cdot \pi/180
\end{aligned} \tag{6}$$

Where ϕ is the local latitude. Accurate solar time t_n, time difference e and solar day angle θ_{day} can be expressed as:

$$\begin{aligned}
t_n &= t_s + e/60 + (\lambda - 120)/15 \\
e &= 9.87 \cdot \sin(2\theta_{day}) - 7.53 \cdot \cos(\theta_{day}) - 1.5 \cdot \sin(\theta_{day}) \\
\theta_{day} &= 360 \cdot (d_n - 81)/364 \cdot \pi/180
\end{aligned} \tag{7}$$

Where λ is the local longitude. The scattered radiation intensity I_{dh} is defined by:

$$I_{dh} = \frac{0.5 \cdot I_0 \cdot \sin(\theta_d) \cdot amr(1 - \tau_h)}{amr - 1.31\tau_h} \tag{8}$$

Finally, the stratospheric radiation calculation formula is expressed as:

$$I_d = I_{d0} + I_{dh} \tag{9}$$

2.2. Curved array irradiation model

The solar cell array on the upper surface of the airship is curved, and its curvature is consistent with that of the airship [23]. In order to establish an accurate radiation model, the finite element method is introduced. The entire PV array is divided into micro-elements, which can be regarded as planes, and the sum of all micro-elements receiving radiation is the radiation of the PV array. The airship surface governing equation can be expressed as:

$$F = x^2 + z^2 - f^2(y) \qquad 0 \le y \le L \tag{10}$$

Where L is the axial length of the PV array. The micro-element area dA can be calculated with:

$$dA = d\theta \cdot dy \cdot r \cdot \sqrt{1 + dr^2} \tag{11}$$

Where θ is the laying angle, and r is the radius of the corresponding circular section. The average vector of the micro-element in the body coordinate system can be given by:

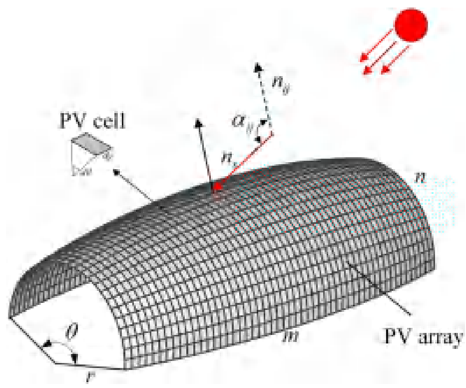

Fig. 2. Finite element model of the PV array.

$$\overrightarrow{n_{ij}} = (n_{ijx}, n_{ijy}, n_{ijz}) = \left(\frac{\partial F}{\partial x}, \frac{\partial F}{\partial y}, \frac{\partial F}{\partial z}\right) \Big/ \sqrt{\left(\frac{\partial F}{\partial x}\right)^2 + \left(\frac{\partial F}{\partial y}\right)^2 + \left(\frac{\partial F}{\partial z}\right)^2} \tag{12}$$

Transformation matrix from body coordinate system to inertial coordinate system can be given by:

$$R = \begin{bmatrix} C_\theta C_\psi & S_\theta C_\psi S_\phi - S_\psi C_\phi & S_\theta C_\psi C_\phi + S_\psi S_\phi \\ C_\theta S_\psi & S_\theta S_\psi S_\phi + C_\psi C_\phi & S_\theta S_\psi C_\phi - C_\psi S_\phi \\ -S_\theta & C_\theta S_\phi & C_\theta C_\phi \end{bmatrix} \tag{13}$$

Where ϕ, θ, and ψ are the roll angle, pitch angle, and yaw angle in the body coordinate system [24]. The microelement average vector in the body coordinate system and the irradiation vector in the inertial frame $\overrightarrow{n_s}$ can be expressed as:

$$\begin{aligned} &(n_{ijIx}, n_{ijIy}, n_{ijIz})^T = R \cdot (n_{ijx}, n_{ijy}, n_{ijz})^T \\ &\overrightarrow{n_s} = (-\cos\theta_{HS} \cdot \cos\theta_{AS}, -\cos\theta_{HS} \cdot \sin\theta_{AS}, -\sin\theta_{HS}) \end{aligned} \tag{14}$$

The angle between the irradiation vector and the microelement normal vector can be expressed as [25]:

$$\alpha_{ij} = cos^{-1}\left(\frac{\vec{n}_{ijI} \cdot \vec{n}_s}{|\vec{n}_{ijI}| \cdot |\vec{n}_s|}\right) \tag{15}$$

As shown in Fig. 2, when the angle between the irradiation vector and the microelement normal vector is obtuse, the radiation intensity of the microelement is the absolute value of the dot product of the two; when the angle is acute, the irradiance value of the microelement is 0. The intensity of direct radiation I_{ij0} and scattered radiation of microelements I_{ijh} can be expressed as:

$$\begin{aligned} &I_{ij0} = \begin{cases} 0 & 0 \le \alpha_{ij} < \dfrac{\pi}{2} \\ |\vec{n}_{ijI} \cdot \vec{n}_s| \cdot I_{d0} & \dfrac{\pi}{2} \le \alpha_{ij} < \pi \end{cases} \\ &I_{ijh} = 0.5 \cdot \left(1 - \frac{n_{ijz}}{|\vec{n}_{ijI}|}\right) \cdot I_{dh} \end{aligned} \tag{16}$$

The total irradiation intensity and irradiation power of the microelement can be given by:

$$P_{ij} = (I_{ij0} + I_{ijh}) \cdot dA_{ij} \tag{17}$$

2.3. Solar cell thermal model

The multilayer structures of PV array from top to bottom are thin-film solar cell, adhesive film, intermediate layer and thermal insulation layer [26]. The energy equation of the thin-film battery layer can be expressed as:

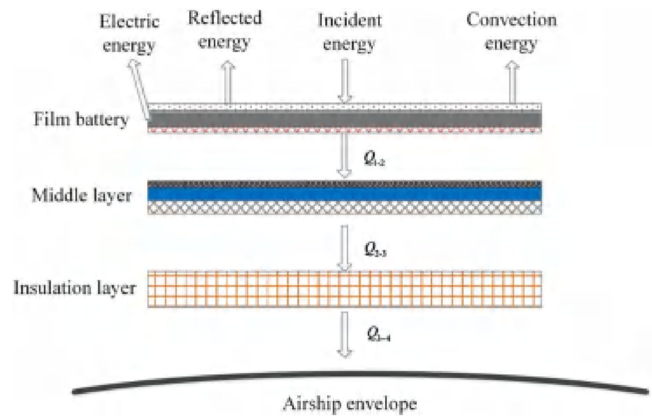

Fig. 3. Schematic diagram of heat transfer of solar cells.

$$\begin{aligned} &m_1 c_1 \frac{dT_1}{dt} = Q_{d0} + Q_{dh} - Q_{out} - Q_{IR} - Q_{12} \\ &Q_{out} = h_{out} \cdot (T_1 - T_{airh}) \\ &Q_{IR} = \varepsilon_e \cdot \sigma \cdot (T_1^4 - T_{airh}^4) \end{aligned} \tag{18}$$

where Q_{d0} and Q_{dh} are direct radiation energy and scattered radiation energy respectively, Q_{out} is the external convection heat dissipation, Q_{IR} is the infrared radiation energy, and Q_{12} is the energy transferred from the thin-film cell layer to the adhesive films, see Fig. 3. ε_e is the infrared emissivity with a value of 0.75 [6]. σ is Stephen Boltzmann's constant. The energy equations of other layers can be given by:

$$\begin{aligned} &m_n c_n \frac{dT_n}{dt} = Q_{n-1,n} - Q_{n,n+1} \\ &Q_{n,n+1} = (T_n - T_{n+1}) / \left(\frac{\delta_n}{\lambda_n} + \frac{\delta_{n+1}}{\lambda_{n+1}}\right) dA \end{aligned} \tag{19}$$

Where m_n, c_n, δ_n and λ_n are the mass, specific heat capacity, thickness, and thermal conductivity of the *nth* layer material, respectively. The temperature of each layer of PV array can be given by:

$$T_n = T_{n0} + \int_0^t dT_n \tag{20}$$

An empirical formula for the efficiency of single-crystal silicon solar cells as a function of temperature is given by:

$$\eta_{ij} = 0.22 - 8.3e^{-4} \cdot (T_1 - 250) \tag{21}$$

The thermal effect on the power output of PV array is shown in Fig. 4. In summary, the output power of the PV array can be expressed as:

$$P_{PV} = \sum_{i=1}^{m} \sum_{j=1}^{n} \eta_{ij} P_{ij} \tag{22}$$

2.4. Required power model

As shown in Fig. 5, the stratospheric airship energy system is mainly composed of PV array, energy storage batteries, energy management systems and loads [27]. The total output power of airship can be expressed as:

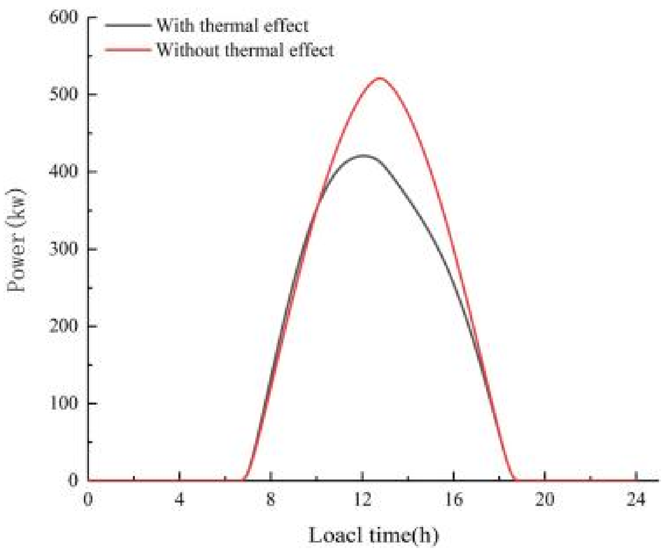

Fig. 4. Thermal effect on output power of PV array.

$$P_{total} = P_{prop} + P_{avio} + P_{meas} + P_{load} \tag{23}$$

Where P_{avio} is the power of the avionics system, P_{meas} is the power of the measurement and control system, and P_{load} is the power of the load system, merge them into P_{others}. Propulsion system power P_{prop} can be given by:

$$P_{prop} = F_T v_{airspeed}/(\eta_{prop}\eta_{mot}) \tag{24}$$

Where η_{prop} is the propeller efficiency, and η_{mot} is the motor efficiency. The thrust of the airship propulsion system can be expressed as:

$$F_T = \frac{1}{2}\rho_{airh} S_{ref} C_D v_{airspeed}^2 \tag{25}$$

Where $v_{airspeed}$ is the airspeed of airship, S_{ref} is the cross-sectional area at the maximum shaft diameter, and C_d is the drag coefficient. The airspeed $v_{airspeed}$ of airship can be expressed as the vector sum of the ground speed of the airship and the local wind speed:

$$\vec{v}_{airspeed} = \vec{v}_{ship} + \vec{v}_{wind} \tag{26}$$

3. Position energy storage strategy

The traditional airship station-keeping strategy is fixed-point (FP) with constant airspeed during day and night [28,29]. Obviously, in the airspace with high wind speed, the FP strategy cannot fulfill the requirements of long-endurance missions. Similar to the gravity potential flight strategy for solar-powered aircraft [19,30], the position energy storage strategy (PES) can store extra energy during the daytime in the wind field potential energy to improve the wind resistance and endurance.

As shown in Fig. 6, the airship flies to the upper wind area at high speed by supplying surplus solar energy to the propulsion system during daytime and reduces the propulsion power to float back to the original position at an airspeed below the wind speed during nighttime. Therefore, it is feasible to increase the utilization rate of solar energy and the average airspeed of the airship through the PES strategy. Besides, the location energy storage strategy is closely related to wind speed and irradiation intensity, so it is necessary to establish a flight strategy model and an energy management model to cope with various environmental conditions.

3.1. Flight strategy model

The core of the PES strategy is to determine the daytime airspeed, and nighttime airspeed. Since the propulsion power has a cubic relationship with the airspeed of the airship, maintaining a constant speed can maximize the average airspeed when the available energy is constant [31]. As shown in Fig. 6, the airship flight phase of PES strategy can be expressed as:

Stage 1: Fly backward at low airspeed V_{night}

Stage 2: All solar energy is used to accelerate the airship.

Stage 3: The airship flies to the upper wind area at airspeed V_{day}. Meanwhile, the excess energy charges the energy storage battery.

Stage 4: As the intensity of solar radiation decreases, the airship decelerates.

Stage 5: The airship floats back to the starting point at airspeed V_{day}.

The change in solar energy and the power required for the airship are shown in Fig. 7, t_1 and t_2 are the acceleration start time and end time, while t_4 and t_5 are the deceleration start time and end time, respectively. Therefore, the cruising speed of the airship $V_{airship}$ can be expressed as:

$$V_{airspeed} = \begin{cases} V_{night} & if\, t_0 \le t < t_1 \\ (\frac{2(P_{PV} - P_{others})\eta_{prop}}{\rho_{airh} C_D S_{ref}})^{\frac{1}{3}} & if\, t_1 \le t < t_2 \\ V_{day} & if\, t_2 \le t < t_4 \\ (\frac{2(P_{PV} - P_{others})\eta_{prop}}{\rho_{airh} C_D S_{ref}})^{\frac{1}{3}} & if\, t_4 \le t < t_5 \\ V_{night} & if\, t_5 \le t < t_{end} \end{cases} \tag{27}$$

Airspeed at nighttime is mainly determined by energy storage battery capacity. The maximum airspeed at night can be expressed as:

$$V_{nightmax} = (\frac{2(Q_{nightmax} - P_{others}\Delta t_{night})\eta_{prop}}{\rho_{airh} C_D S_{ref} \Delta t_{night}})^{\frac{1}{3}} \tag{28}$$

Where Δt_{night} is nighttime and $Q_{nightmax}$ is the maximum available energy during nighttime, which can be calculated by:

$$Q_{nightmax} = \eta_{depth}\eta_{discharge} E_{battery} + \int_{sunrise}^{t_1} P_{PV} dt + \int_{t_4}^{sunset} P_{PV} dt \tag{29}$$

Where η_{depth} is discharge depth of battery, and $\eta_{discharge}$ is discharge efficiency of battery. The forward distance during the daytime needs to balance the backward distance during night time. Besides, in order to ensure enough surplus energy to charge the energy storage battery, it is necessary to set the maximum airspeed. The airspeed during daytime V_{day} can be given by:

$$V_{day} = \begin{cases} V_{req} & if\, V_{req} \le V_{daymax} \\ V_{daymax} & if\, V_{req} > V_{daymax} \end{cases} \tag{30}$$

Where V_{req} is the required airspeed at daytime, and V_{daymax} is maximum available airspeed. When Q_{charge} and $\eta_{depth} E_{battery}$ are equal, the corresponding airspeed is V_{daymax}. In order to achieve regional residence within the scope through the PES strategy, optimization goal can be given by:

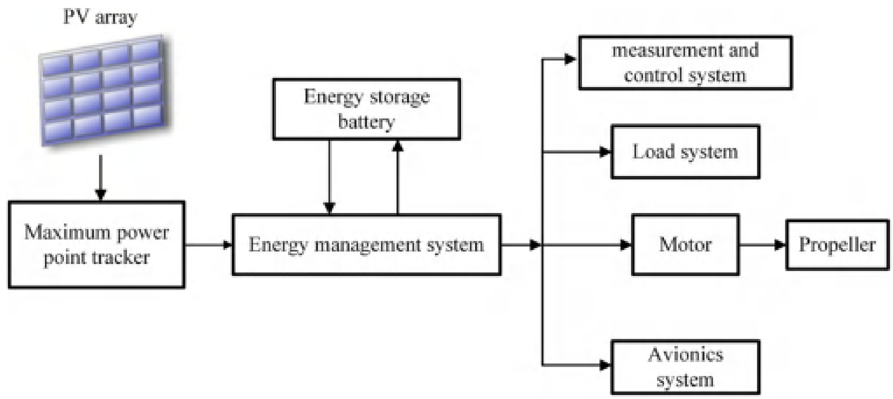

Fig. 5. Renewable energy system of stratospheric airship.

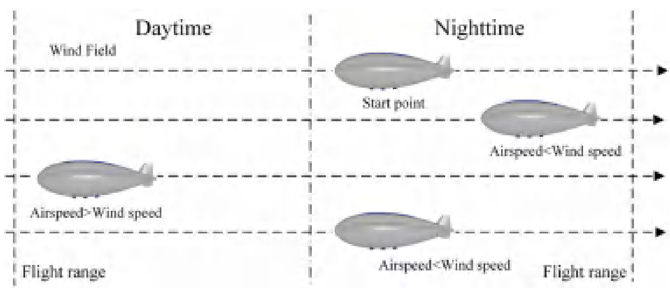

Fig. 6. Schematic diagram of PES strategy.

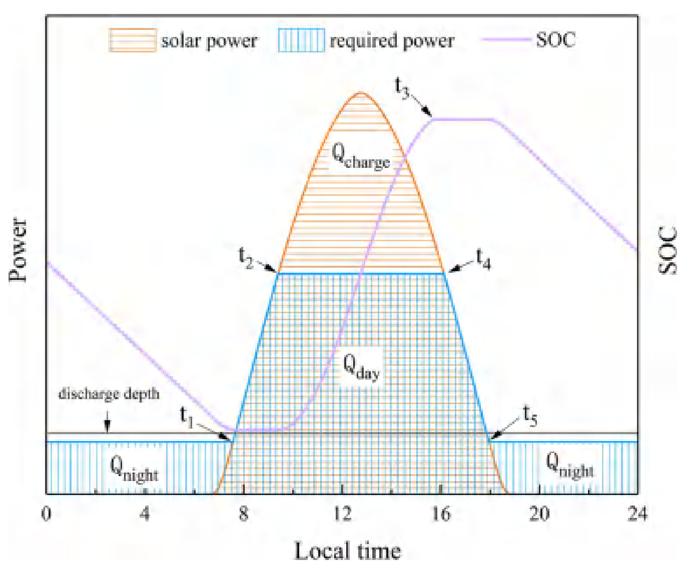

Fig. 7. Energy balance based on PES strategy.

$$\textbf{goal}: \quad min\,(S_{start} - S_{end}) \tag{31}$$

According to Eq.

$$V_{airspeed} = \begin{cases} V_{night} \quad if\, t_0 \le t < t_1 \\ (\dfrac{2(P_{PV} - P_{others})\eta_{prop}}{\rho_{airh} C_D S_{ref}})^{\frac{1}{3}} \quad if\, t_1 \le t < t_2 \\ V_{day} \quad if\, t_2 \le t < t_4 \\ (\dfrac{2(P_{PV} - P_{others})\eta_{prop}}{\rho_{airh} C_D S_{ref}})^{\frac{1}{3}} \quad if\, t_4 \le t < t_5 \\ V_{night} \quad if\, t_5 \le t < t_{end} \end{cases}$$

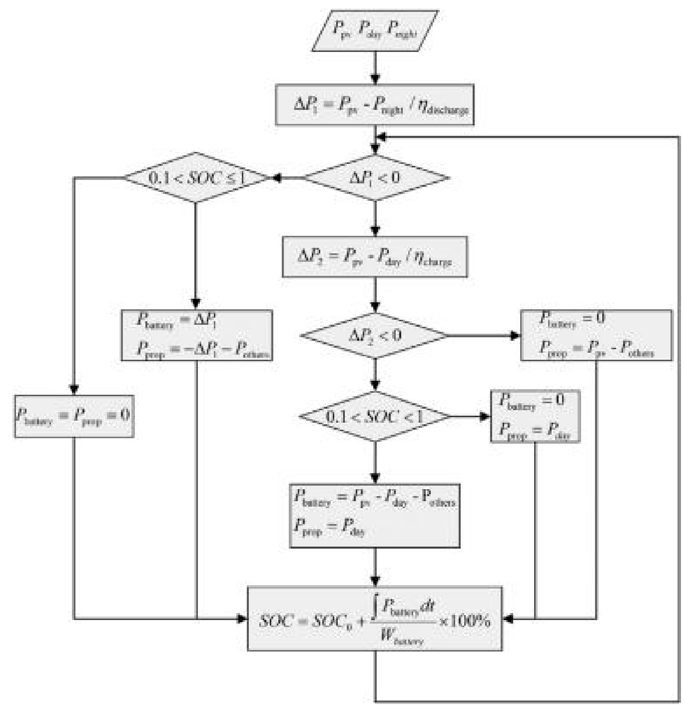

Fig. 8. Flow chart of energy management.

(27) and $V_{nightmax} = (\frac{2(Q_{nightmax} - P_{others}\Delta t_{night})\eta_{prop}}{\rho_{airh} C_D S_{ref} \Delta t_{night}})^{\frac{1}{3}}$ (28), optimization goals can be translated into:

$$\textbf{goal}: \quad min(V_{day}(t_4 - t_2) + \int_{t_1}^{t_2} V_{airspeed} dt + \int_{t_3}^{t_4} V_{airspeed} dt - V_{nightmax}(24 - t_5 + t_1)) \tag{32}$$

3.2. Energy management model

In order to achieve the flight strategy, an energy management model based on the PES strategy is established, as shown in Fig. 8. The total power consumed by the airship can be expressed as:

$$\begin{aligned} P_{day} &= \frac{1}{2}\rho_{airh} C_D S_{ref} V_{day}^3 + P_{others} \\ P_{night} &= \frac{1}{2}\rho_{airh} C_D S_{ref} V_{night}^3 + P_{others} \end{aligned} \tag{33}$$

Table 1
Airship parameters.

Geometric Parameter		Energy system parameter	
Length, m	220	Efficiency of solar cells (273 K)	0.2
Diameter, m	54	Battery energy density, Wh/kg	330
Envelope area, m^2	33000	Center angle of PV array, °	90
Volume, m^3	380000	Efficiency for motor	0.93
Ceiling altitude, m	20000	Efficiency for propeller	0.77
PV array area, m^2	2200	Battery capacity, kWh	700

According to Eq.

$$V_{airspeed} = \begin{cases} V_{night} \quad if\, t_0 \le t < t_1 \\ \left(\dfrac{2(P_{PV} - P_{others})\eta_{prop}}{\rho_{airh} C_D S_{ref}}\right)^{\frac{1}{3}} \quad if\, t_1 \le t < t_2 \\ V_{day} \quad if\, t_2 \le t < t_4 \\ \left(\dfrac{2(P_{PV} - P_{others})\eta_{prop}}{\rho_{airh} C_D S_{ref}}\right)^{\frac{1}{3}} \quad if\, t_4 \le t < t_5 \\ V_{night} \quad if\, t_5 \le t < t_{end} \end{cases}$$

(27) and $\begin{matrix} P_{day} = \frac{1}{2}\rho_{airh} C_D S_{ref} V_{day}^3 + P_{others} \\ P_{night} = \frac{1}{2}\rho_{airh} C_D S_{ref} V_{night}^3 + P_{others} \end{matrix}$ (33), the energy management model can be represented explicitly in Fig. 10. Further, the function of SOC over time can be calculated by:

$$SOC = \begin{cases} SOC_0 - \int_{t_0}^{t_1} \frac{(P_{night}/\eta_{discharge} - P_{PV})}{E_{battery}} dt \quad if\, t_0 \le t < t_1 \\ 0.1 \quad t_1 \le t < t_2 \\ 0.1 + \int_{t_2}^{t_3} \frac{(P_{PV} - P_{day})}{\eta_{charge} E_{battery}} dt \quad if\, t_2 \le t < t_3 \\ 1 \quad if\, t_3 \le t < t_5 \\ 1 - \int_{t_0}^{t_1} \frac{(P_{night}/\eta_{discharge} - P_{PV})}{E_{battery}} dt \quad if\, t_5 \le t < t_{end} \end{cases} \quad (34)$$

Where SOC_0 is the value at the initial time, η_{charge} and $\eta_{discharge}$ are the charging efficiency and discharging efficiency, respectively.

4. Result and discussion

In this section, in order to analyze the impact of location energy storage strategy on airship endurance performance, firstly, the airship energy harvesting and output are discussed. Meanwhile, taking Sanya as a case, an analysis of PES strategy is carried out. Finally, the impact of PES strategy on energy system configuration under different flight environments is analyzed. The basic parameters of stratospheric airship are listed in Table 1.

4.1. Energy harvesting and consumption analysis

During the long-endurance station-keeping of the airship, latitude, date, and yaw angle will have a significant impact on solar energy. Therefore, it is crucial to evaluate energy harvesting by airships. The daily production capacity of PV array per unit area throughout the year in China is shown in Fig. 9 and Fig. 10.

At low latitudes, the solar energy changes steadily within one year, with the highest in summer solstice and the lowest in the winter solstice. When the yaw angle is 0°, the annual output energy varies from 1550 Wh/m^2 to 1750 Wh/m^2. Compared to low latitudes, solar energy in high latitudes is slightly higher in summer and significantly lower in winter, and the difference reached 1250 Wh/m^2. From May to August, the radiant energy value is higher in the high latitude regions, while the radiant energy value is higher in the low latitude regions in the rest of months.

For the 90° yaw angle, from Fig. 10, the annual changes in solar energy have the same trend as the 0° yaw angle, while the year-round solar energy is significantly lower. The irradiation input in

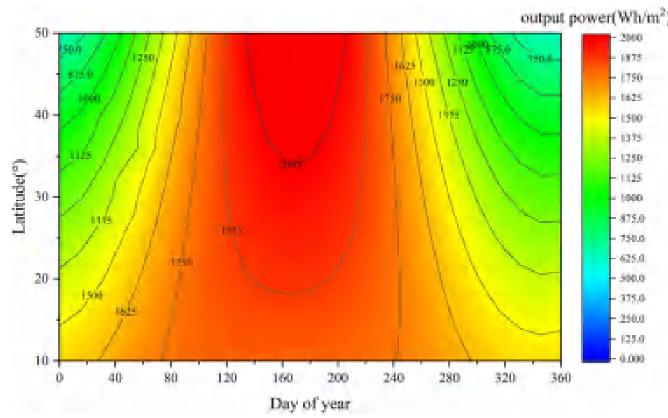

Fig. 9. The contour maps of output energy of unit area solar array on 0° yaw angle. (For interpretation of the colors in the figure(s), the reader is referred to the web version of this article.)

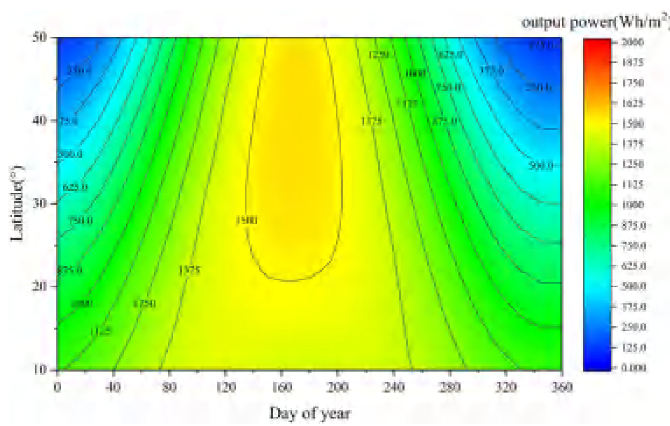

Fig. 10. The contour maps of output energy of unit area solar array on 90° yaw angle.

summer is reduced by about 400 Wh/m^2, while the difference in winter is even higher, reaching 500 Wh/m^2. This occurs due to the sun rises from the east to the west, and the solar cells are arranged along with the airship longitudinally, resulting in a larger average incidence angle of the north-south direction radiation vector. In winter, as the altitude angle of the sun becomes smaller, the variation of the incident angle of the irradiation vector has a more significant effect on solar energy.

Compared with traditional aircraft, airships have large inertia and windward area and low cruise speed. The influence of wind field on energy consumption of the airship is another critical factor of energy balance. As shown in Fig. 11, increasing the angle of attack and sideslip will increase the drag coefficient sharply. Fig. 12 shows the change of airship propulsion power with airspeed at different sideslip angles. When the sideslip angle is 10°, the propulsion power is doubled, and when the sideslip angle is 40°, it is increased by 40 times. Obviously, the effect of the sideslip angle on the airship energy balance is much higher than the effect

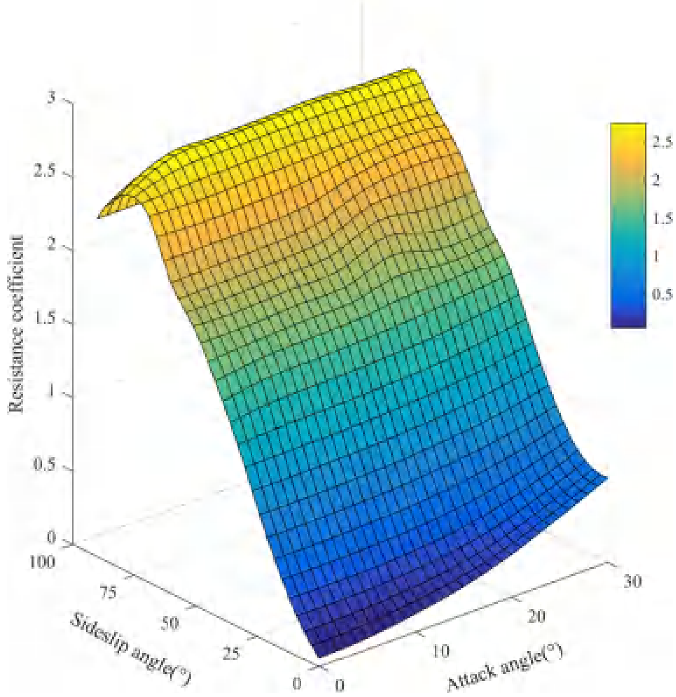

Fig. 11. Airship drag coefficient changes with the angle of attack and sideslip angle.

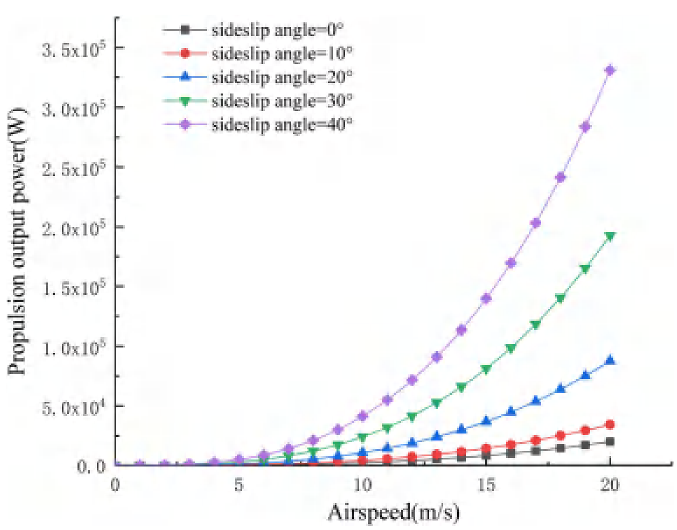

Fig. 12. Airship propulsion power varies with sideslip angle.

of the yaw angle. Although flying at a 0° yaw angle will increase the PV array capacity to a certain extent, considering the additional consumption of propulsion power, the airship should maintain a 0° side slip angle to resist wind. The stratospheric wind direction is usually east-west. Since the stratospheric wind field is usually east-west, the 90° yaw angle should be used as the basis for the design of the PES strategy.

4.2. Case study

According to Section 4.1, at the low latitudes, the annual radiation changes are more gentle. Therefore, the regular dates in the Hainan region (spring, summer, autumn, and winter solstice) are selected as the study case. The daily average wind field data corresponding to the date is shown in Table 2. The simulation period is 48 h. The value of soc at the beginning of the simulation is 0.65.

Table 2
Average daily wind speed and direction in Hainan on different days.

Date	Wind speed (m/s)	Wind direction (°)
Spring equinox	16.1	280
Summer solstice	21.5	80
Autumn equinox	17.4	90
Winter solstice	10.5	265

The results of energy balance history are shown in Fig. 13, where the red line represents solar input energy, the blue line represents the total power consumed by the airship, and the green line is the SOC of energy storage battery. On the winter solstice, due to the low wind speed, the airship can be stationed at a fixed airspeed (FP strategy), the total power is constant at 17.3 kw, as shown in Fig. 13(b). The energy storage battery is far from the depth of discharge, and the minimum SOC reaches only 0.6 in the second night. The lowest SOC is 0.6 on the second night time, far from reaching the discharge depth. During most of the day, the energy storage battery is fully charged.

However, for seasons with high wind speeds, the FP strategy cannot meet the requirements of long-term regional station-keeping missions, so the PES strategy is necessary. According to Fig. 13(a), on the spring equinox, the airship recedes at 15 m/s airspeed at night and starts accelerating to 8.25 h at 8.07 h, reaching 17.8 m/s airspeed and flying forward at constant airspeed until 17.5 h, decelerating to 15.1 m/s at 17.8 h, finally float back to the initial position. During the whole process, the battery is charged from 8.25 h to 11.5 h, and maintains a full charge state until 16 h. Similar to spring equinox, the wind field in autumn equinox is larger. In order to balance the retreat distance at night, the airspeed during the day is higher, reaching 20.8 m/s; meanwhile, the battery full charge time is delayed to 12 h. As shown in Fig. 14, on the vernal equinox and summer solstice, the flight ranges of the airship are 52 km and 112 km, respectively, which are acceptable for gigantic stratospheric airships performing communication relay missions.

As to summer solstice, the results of energy and power history are represented in Fig. 13(b), the airspeed and distance history is represented by the red lines in Fig. 14. The airship begins to fly backward at a 15.5 m/s airspeed until 7.4 h, then all the solar energy is used for acceleration. After reaching the daytime airspeed of 26.9 m/s at 8.8 h, the airship keeps the constant speed to 16.3 h and then decelerates to the airspeed of 15.5 m/s due to the weakening of irradiation intensity. It can be seen that in a 24-hour energy cycle, the utilization rate of solar energy reaches 100%. Although all solar energy is used for propulsion and energy storage, the airship still shifts 300 km from the initial position during the 48 h simulation. It is because the PES strategy is to improve the wind resistance by adjusting the day and night energy distribution, but the total energy is constant. The summer solstice wind speed exceeds the upper limit of the airship design average airspeed.

It can be seen that even if the PES strategy is adopted, the airship cannot achieve long-term station-keeping on the date when the wind speed exceeds the available airspeed of the airship. Therefore its applicability needs to be discussed. Fig. 15 shows the maneuver strategy corresponding to the Hainan wind field throughout the year, where green dots, red dots and blue dots represent FP strategy, PES strategy and MFS strategy, respectively. It can be inferred that the energy shortage in the night from January to June and September is solved by the PES strategy. In June-August, wind speed is between available airspeed and maximum airspeed most of the time, so it is almost impossible to perform long-term missions. However, for short-term reconnaissance missions in fixed areas, it is possible to increase the endurance by

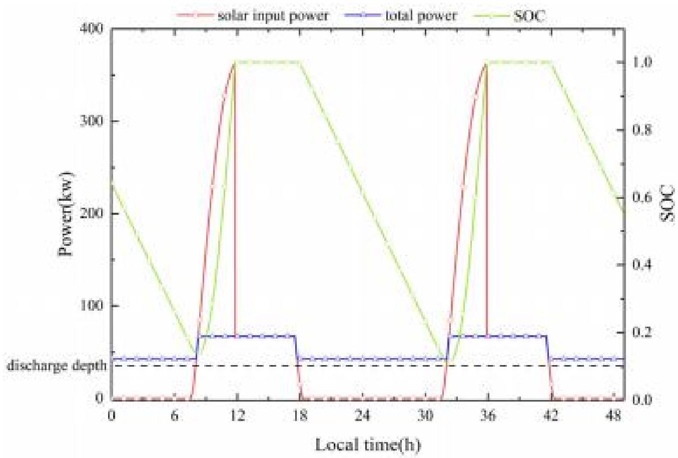

(a) Spring equinox

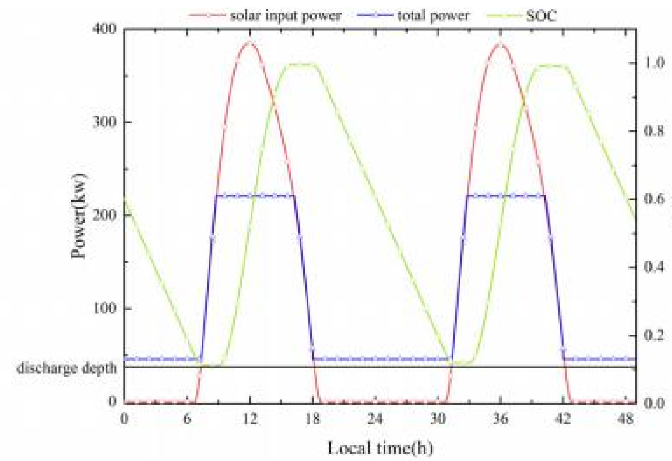

(b) Summer solstice

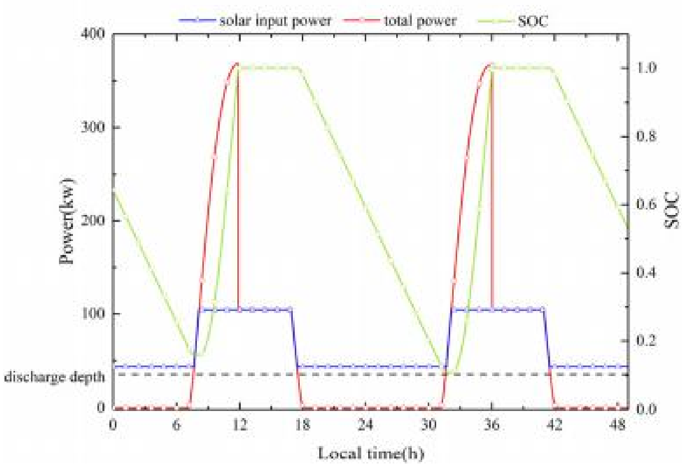

(c) Autumn equinox

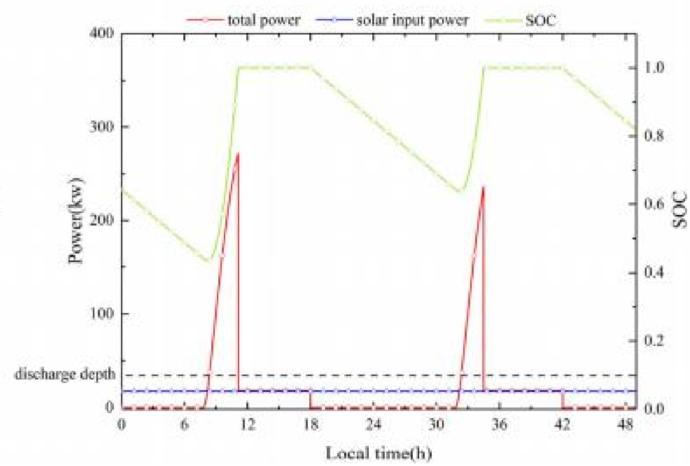

(d) Winter solstice

Fig. 13. Energy balance history on different dates in Hainan.

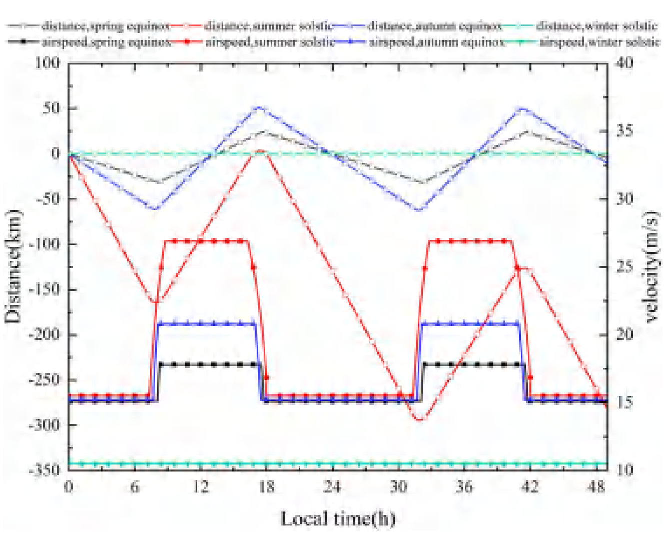

Fig. 14. Distance and airspeed history on different dates in Hainan.

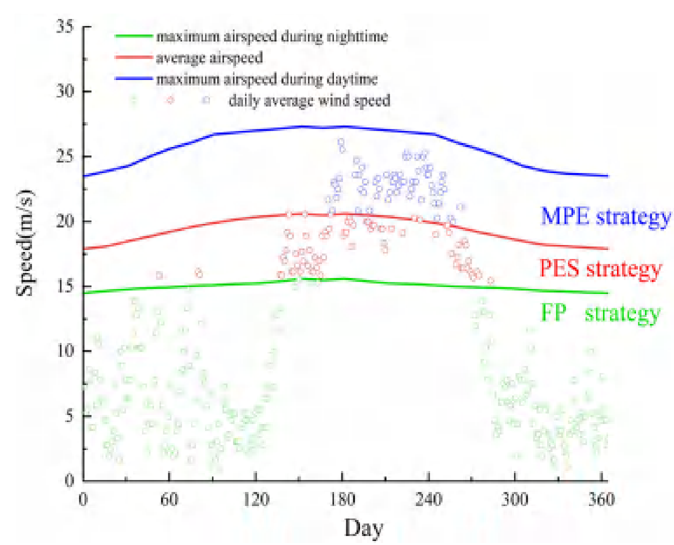

Fig. 15. Maneuvering strategy corresponding to wind speed throughout the year.

increasing the initial position potential and initial electrical energy, which can be called maximum potential energy (MPE) strategy.

Take the summer solstice as an example, and the radius of the mission area is 150 km. The distance history of the airship with different initial conditions is shown in Fig. 16. When the initial SOC is 0.6, the airship flies back quickly and floats out of the mission range at 6.94 h, as shown by the black line. When the initial SOC increases to 0.8, the available airspeed on the first night increases, and the retreat distance decreases, resulting in a signif-

Table 3
Monthly average wind seed over cities of different latitudes in China (m/s).

City	Latitude	JAN	FEB	MAR	APR	MAY	JUN	JUL	AUG	SEP	OCT	NOV	DEC
Sanya	18.31	11.6	13.1	16	8	15.56	19.2	24.5	23	18.7	14.6	13	11
Haikou	20.03	11.56	14.3	11.2	13.33	14.56	18.36	19	20.1	17.46	9.6	7.22	11.66
Hongkong	22.2	13.66	14.6	12.36	12.03	13.3	17.43	18.7	19.4	16.36	8.73	9.16	14.2
Guangzhou	23.62	16.2	17.6	12.8	12.2	11.03	17.2	18.5	18.76	13.16	8.63	10.03	15.9
Fuzhou	26.08	18.6	18.4	14.8	12.46	9.2	14.4	16.2	17.73	12.96	9.9	14.9	18.9
Changsha	28.23	20.6	18.9	15.8	13	9.3	12.1	18.1	19.46	12.5	11.6	16.2	24.8
Wuhan	30.6	24.9	22.1	15.56	14.2	10.5	11.6	17.6	17.1	11.5	12.7	19.4	28.1
Nanjing	32.07	30.3	25.1	16.9	14.8	11.1	11.83	17.7	15.76	12.6	14.1	20.2	29
Xian	34.27	31.8	23.76	15	15.46	13.7	12.7	16.2	14.2	13.13	14.9	21.1	24.4
Lanzhou	36.07	35.5	26.2	15.7	14.7	13.73	13.13	13.56	11.55	12.3	16.1	21.9	24.5
Taiyuan	37.97	35.6	25.6	18.43	17.6	13.33	14.43	12.53	10.43	12.1	14.03	24.1	27.03
Beijing	39.93	38.3	23.8	20.03	20.7	14.8	10.3	10	9.6	12.83	14.7	22.5	31.4
Shenyang	41.84	37	24.3	21.53	10.3	15.3	10.2	8.63	10.5	11	13.3	22.9	32.6
Wulumuqi	43.82	35.7	25.8	24.9	20.4	14.3	10.5	8.4	9.6	11.5	16.2	21.7	20.9
Haerbin	45.89	35.1	23.3	23	20.2	16.2	13.16	9	12.6	13.1	11	22	28.5

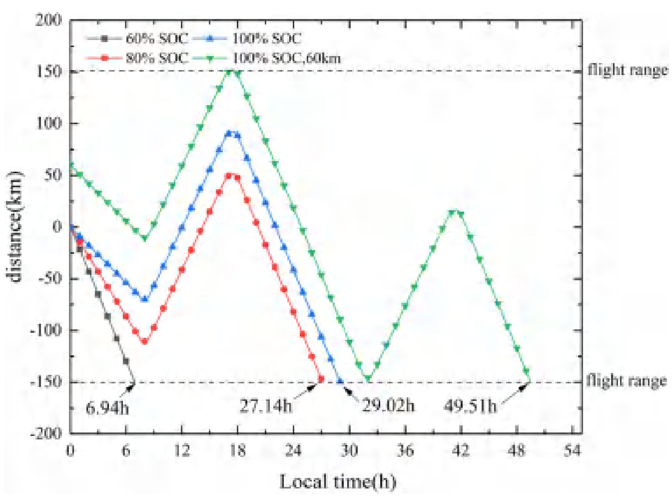

Fig. 16. Displacement history under different initial conditions.

icant increase in the endurance to 24.14 h. Further, endurance increases to 29.02 h when the initial SOC is 1. As shown by the blue line, the airship does not reach the upper boundary of airspace, and part of the position potential energy is wasted. In order to fully exploit position potential, the initial position is set to 60 km. The airship reaches the mission airspace boundary at 15 h and 31.7 h, and finally, flows out of the mission range at 49.51 h, whose endurance is increased by 58% compared with the initial position of 0 km. Therefore, it is feasible to pre-store excess position potential energy in the previous day to enhance the ability to resist short-term high-speed wind fields.

4.3. Impact of PES strategy on energy system configuration

According to Section 4.1, the PES strategy can solve the problem of energy shortage in some months. The wind speeds in the month change considerably different latitudes, as shown in Table 3, besides, flight airspace is another limitation to PES strategy. Therefore, this section mainly discusses the impact of PES on airship energy system configuration under different airship flight conditions.

4.3.1. Impact of airspace position and range

Energy system configuration changes with airspace range and average wind speed. In the middle and high latitudes, the irradiation intensity is low in January and December, and the wind speed is tremendous, which is not suitable for airship flight [16]. Therefore, select February to November for analysis.

Fig. 17 shows the mass of the energy system in different airspace ranges, where the green and red bars represent the PV array mass and the energy storage battery mass, respectively. It can be seen that compared with the FP resident strategy, using the PES strategy as a design basis can reduce the total mass of energy system to varying degrees. In the summer at low latitudes, when the flight range is 100 km, 200 km, and 300 km, the total mass of the energy system decreases by 7.5%, 19.7%, and 29.2%, respectively, while this value is only 2.4%, 4.6%, and 4% in winter at low latitudes. This is due to the low radiation intensity in autumn and winter in high latitude areas, which is the main factor limiting the airship's wind resistance, not the battery capacity. Therefore, the PES strategy is more suitable for areas with high irradiation intensity.

Moreover, the PES strategy can significantly reduce the mass of the energy storage battery, and at the same time, the mass of the PV array will increase to a certain extent. When the average wind speed is the same, compared with the FP strategy, the PES strategy will lead to an increase in the total energy required due to the difference in day and night speed, which needs to be considered in the baseline design of the airship.

4.3.2. Impact of wind speed

From May to July, as the latitude increases, although the irradiated energy is relatively close, the wind speed is gradually decreasing, as shown in Fig. 10 and Table 3. Fig. 18 shows the energy system quality corresponding to different wind speeds when the irradiation intensity is fixed. At the designed wind speed of 10 m/s, the maximum mass reduction of the energy system is only 7.9%, so the fixed-point residence strategy is more suitable. However, at wind speeds of 15 m/s, the PES strategy in 100 km airspace has more advantages. At wind speeds of 20 m/s and above, the mass reduction effect of the 300 km PES strategy is most apparent. The higher the average airspeed, the more advantageous the PES strategy. It can be speculated that as the airspace increases, the location energy storage strategy can reduce the quality of the energy system more, but the airspace range cannot be increased indefinitely, and 300 km is a more reasonable planned airspace range.

4.3.3. Effect of battery energy density

The relatively low energy density of lithium batteries is one of the main factors affecting the long-term station-keeping of airships. Renewable fuel cells, due to their ultra-high energy density, can replace lithium batteries in the future as a better choice for airship energy storage systems [32][33].

A comparison of the batteries with varying energy density is conducted in this study, as shown in Fig. 19 With the energy density of energy storage batteries increasing, the total mass of energy system continues to decrease. When the energy density of battery

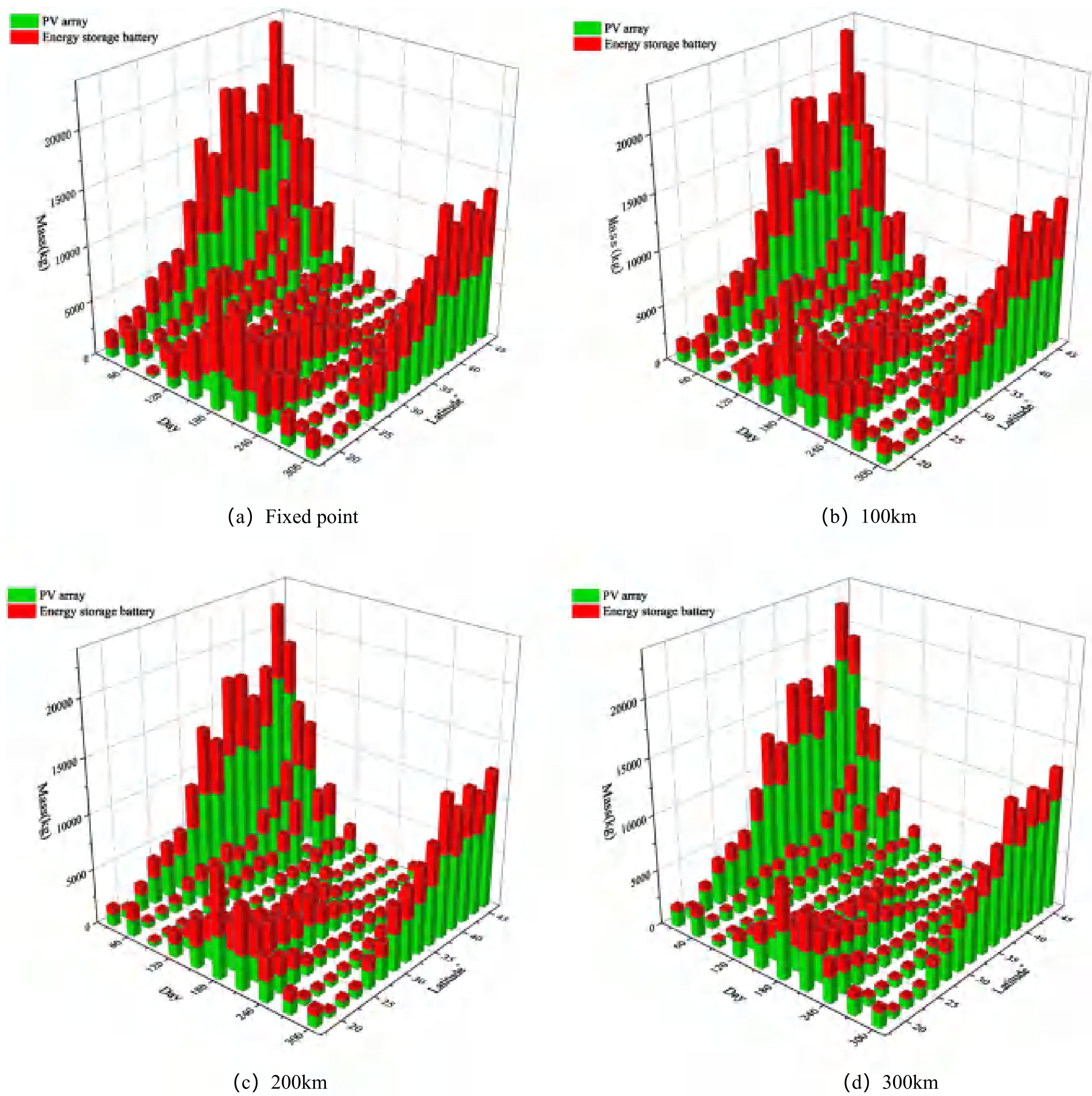

Fig. 17. Stratospheric airship energy system configuration under different airspace ranges.

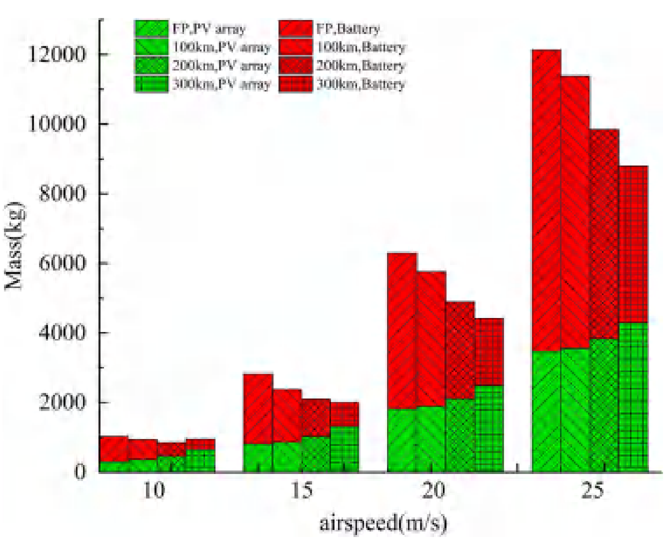

Fig. 18. Energy system configuration at different wind speeds.

is low, the PES strategy can significantly reduce the mass of energy system, especially during the high wind speeds of June to September. With the increase of energy density, the advantage of the PES strategy is weakened. When the energy density of battery reaches 1000 wh/kg, the mass gap of energy system with different strategies maneuver is small, while the PES strategy of 100 km range is still the optimal strategy in most months.

Besides, it is worth noting that PES strategy of 300 km will increase the total quality of energy system in some months whose wind speed is relatively low. This occurs due to the PV array has become the dominant factor affecting the mass of the energy system, causing that the excessively large diurnal speed difference results in the mass of PV array to an additional increase.

5. Conclusion

In this paper, a maneuvering strategy and an energy management strategy for stratospheric airships based on position energy storage are proposed, and the feasibility is analyzed through a case. Moreover, the energy system configuration problem based on the PES strategy is studied, which has certain value for the design of

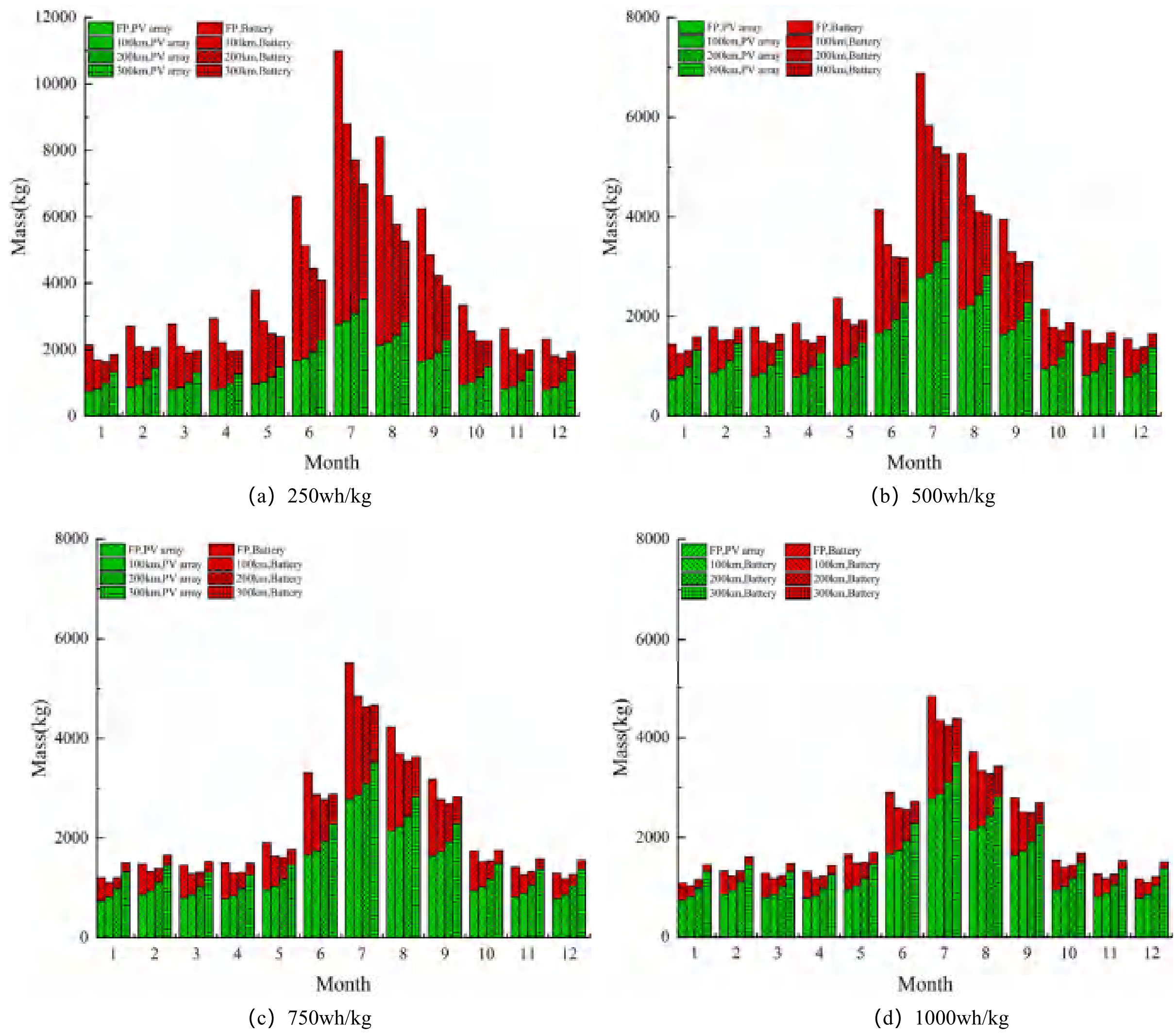

(a) 250wh/kg (b) 500wh/kg (c) 750wh/kg (d) 1000wh/kg

Fig. 19. Comparison of energy system mass under different energy densities of battery.

stratospheric airships The main conclusions can be summarized as follows:

(1) By balancing the energy input and output of the airship, the east-west course should be used as the design basis.
(2) The night energy shortage problem in Hainan from January to June and September can be solved by PES strategy.
(3) On summer solstice when the available airspeed is less than the wind speed, the endurance time can be increased from 6.94 h to 49.51 h by pre-storing position potential and electrical energy.
(4) Taking the PES strategy as the design basis can reduce the total mass of the energy system, and has more advantages in areas with higher irradiation energy density and higher wind speed.

Declaration of competing interest

There is no conflict of interest.

Acknowledgements

This work was supported by the National Natural Science Foundation of China under Grant No. 51775021, the Fundamental Research Funds for the Central Universities under Grant No. YWF-18-BH-Y-165, Key Laboratory of Aircraft Advanced Design Technology (Beihang University) Ministry of industry, the fifth youth top talent support program of Beihang University.

References

[1] F.A. Oliveria, F.C. Lourenco, T.C. Devezas, High-altitude platforms - present situation and technology trends, J. Aerosp. Technol. Manag. 8 (2016) 249–262.
[2] T.A. Ozoroski, C.L. Nickol, M.D. Guynn, High altitude long endurance UAV analysis model development and application study comparing solar powered airplane and airship station-keeping capabilities, 2015, NASA/TM-2015-218677.
[3] A. Colozza, PV/regenerative fuel cell high altitude airship feasibility study, in: 2nd AIAA "Unmanned Unlimited" Systems, Technologies, and Operations, 2003.
[4] H. Wang, B. Song, L. Zuo, Effect of high-altitude airship's attitude on performance of its energy system, J. Aircr. 44 (2007) 77–80.
[5] J.H. Shi, X.J. Zhu, S. Sui, Modeling and analysis of solar energy collected by stratosphere airship's surface, Comput. Simul. 24 (2007) 64–67.
[6] Jun Li, Mingyun Lv, Dongjie Tan, Weiyu Zhu, Kangwen Sun, Yuanyuan Zhang, Output performance analyses of solar array on stratospheric airship with thermal effect, Appl. Therm. Eng. 104 (2016) 743–750.
[7] Jun Li, Mingyun Lv, Dongjie Tan, Weiyu Zhu, Kangwen Sun, Simplified analytical model for investigating the output power of solar array on stratospheric airship, Int. J. Aeronaut. Space Sci. 17 (2016) 432–441.
[8] Durlabh Pande, Dries Verstraete, Impact of solar cell characteristics and operating conditions on the sizing of a solar powered nonrigid airship, Aerosp. Sci. Technol. 72 (2018) 353–363.
[9] Huafei Du, Weiyu Zhu, Yifei Wu, Lanchuan Zhang, Jun Li, Mingyun Lv, Effect of angular losses on the output performance of solar array on long-endurance stratospheric airship, Energy Convers. Manag. 147 (2017) 135–144.

[10] Kangwen Sun, Ming Zhu, Simulation analysis for solar array output characteristics on stratospheric airship, in: 2012 IASTED International Conference on Power and Energy Systems and Applications, Las Vegas, USA, 2012.
[11] Guillermo Quesada, Laura Guillon, Daniel R. Rousse, Mostafa Mehrtash, Yvan Dutil, Pierre-Luc Paradis, Tracking strategy for photovoltaic solar systems in high latitudes, Energy Convers. Manag. 103 (2015) 147–156.
[12] M. Rahimi, M. Banybayat, Y. Tagheie, P. Valeh-e-Sheyda, An insight on advantage of hybrid sun–wind-tracking over sun-tracking PV system, Energy Convers. Manag. 105 (2015) 294–302.
[13] Mingyun Lv, Jun Li, Weiyu Zhu, Huafei Du, Junhui Meng, Kangwen Sun, A theoretical study of rotatable renewable energy system for stratospheric airship, Energy Convers. Manag. 140 (2017) 51–61.
[14] Mingyun Lv, Jun Li, Huafei Du, Weiyu Zhu, Junhui Meng, Solar array layout optimization for stratospheric airships using numerical method, Energy Convers. Manag. 135 (2017) 160–169.
[15] Weiyu Zhu, Jun Li, Yuanming Xu, Optimum attitude planning of near-space solar powered airship, Aerosp. Sci. Technol. 84 (2019) 291–305.
[16] Lanchuan Zhang, Jun Li, Yifei Wu, Mingyun Lv, Analysis of attitude planning and energy balance of stratospheric airship, Energy 183 (2019) 1089–1103.
[17] Sai Sudha Ramesh, Kian Meng Lim, Hp Lee, Boo Cheong Khoo, Reduced order modeling of stratospheric winds and its application in high altitude balloon trajectory simulations, J. Appl. Meteorol. Climatol. 56 (2017) 1753–1766.
[18] Xianzhong Gao, Zhongxi Hou, Zheng Guo, Jianxia Liu, Xiaoqian Chen, Energy management strategy for solar-powered high-altitude long-endurance aircraft, Energy Convers. Manag. 70 (2013) 20–30.
[19] Shaoqi Wang, Dongli Ma, Muqing Yang, Liang Zhang, Guanxiong Li, Flight strategy optimization for high-altitude long-endurance solar-powered aircraft based on Gauss pseudo-spectral method, Chin. J. Aeronaut. 32 (10) (2019) 2286–2298.
[20] Xixiang Yang, Duoneng Liu, Conceptual design of stratospheric airships focusing on energy balance, J. Aerosp. Eng. 31 (2018) 04017094.
[21] Xixiang Yang, Duoneng Liu, Renewable power system simulation and endurance analysis for stratospheric airships, Renew. Energy 113 (2017) 1070–1076.
[22] J.A. Foster, G.S. Aglietti, The thermal environment encountered in space by a multifunctional solar array, Aerosp. Sci. Technol. 14 (2010) 213–219.
[23] Huafei Du, Mingyun Lv, Lanchuan Zhang, Weiyu Zhu, Yifei Wu, Jun Li, Energy management strategy design and station-keeping strategy optimization for high altitude balloon with altitude control system, Aerosp. Sci. Technol. 93 (2019) 1–9.
[24] Kangwen Sun, Qinzhen Yang, Yang Yang, et al., Numerical simulation and thermal analysis of stratospheric airship, Proc. Eng. 99 (2015) 763–772.
[25] Qiumin Dai, Xiande Fang, Xiaojian Li, Lili Tian, Performance simulation of high altitude scientific balloons, Adv. Space Res. 49 (2012) 1045–1052.
[26] Huafei Du, Jun Li, Weiyu Zhu, Zhongbing Yao, Erqiang Cui, Mingyun Lv, Thermal performance analysis and comparison of stratospheric airships with rotatable and fixed photovoltaic array, Energy Convers. Manag. 158 (2018) 373–386.
[27] Shi Yin, Ming Zhu, Haoquan Liang, Multi-disciplinary design optimization with variable complexity modeling for a stratosphere airship, Chin. J. Aeronaut. 32 (2019) 1244–1255.
[28] H. Liang, et al., Conceptual design optimization of high altitude airship in concurrent subspace optimization, in: 50th AIAA Aerospace Sciences Meeting Including the New Horizons Forum and Aerospace Exposition, 2012.
[29] Jun Li, Jun Liao, Yuxin Liao, Huafei Du, Shibin Luo, Weiyu Zhu, Mingyun Lv, An approach for estimating perpetual endurance of the stratospheric solar-powered platform, Aerosp. Sci. Technol. 79 (2018) 118–130.
[30] Yu Huang, Jianguo Chen, Honglun Wang, Guofeng Su, A method of 3D path planning for solar-powered UAV with fixed target and solar tracking, Aerosp. Sci. Technol. 92 (2019) 831–838.
[31] Miao Yuhong, Zhou Jianghua, Analysis on the optimal transfer of the stratospheric airship in wind field, in: 2018 37th Chinese Control Conference (CCC), IEEE, 2018.
[32] Jun Liao, Yi Jiang, Jun Li, Yuxin Liao, Huafei Du, Weiyu Zhu, Lanchuan Zhang, An improved energy management strategy of hybrid photovoltaic/battery/fuel cell system for stratospheric airship, Acta Astronaut. 152 (2018) 727–739.
[33] G. Romeo, et al., Design of transport aircraft powered by fuel cell & flight test of zero emission 2-seater aircraft powered by fuel cells fueled byhydrogen, Int. J. Hydrog. Energy 38 (2013) 469–479.